Plasma Frequency Selective Surfaces

Ted Anderson, Igor Alexeff, *Fellow, IEEE*, James Raynolds, Esmaeil Farshi, Sriram Parameswaran, Eric P. Pradeep, *Student Member, IEEE*, and Jyothi Hulloli

***Abstract*—This paper is focused on using plasma as a substitute for metal in a frequency selective surface ("FSS"). FSSs have been used for filtering electromagnetic waves. Each FSS layer has to be modeled using numerical methods, and the layers are stacked in such a way to create the desired filtering. Genetic algorithms are used to determine the stacking needed for the desired filtering. This is a complicated and numerically expensive process. We developed a method to replace metal in an FSS with plasma elements. Our plasma FSSs can be tuned to a desired filtering by varying the density in the plasma elements. This could save much of the routine analysis involved in the standard analysis of the conventional FSS structures. The user simply tunes the plasma to get the desired filtering. Plasma elements offer the possibility of improved shielding along with reconfigurability and stealth. Plasma FSS can be made transparent by turning the plasma OFF. This extends our previous scientific achievements in the development of the plasma antenna.**

***Index Terms*—Active antennas, antennas, plasma antennas, plasma devices.**

I. Introduction

As THE DENSITY of the plasma is increased, the plasma skin depth becomes smaller and smaller until the elements behave as metallic elements, and we create filtering similar to frequency selective surface (FSS) with metallic elements. Up until the metallic mode for the plasma, our theory and experiments showed that the plasma FSS had a continuous change in filtering. We developed a basic mathematical model for a plasma FSS by modeling the plasma elements as half-wavelength and full-wavelength dipole elements in a periodic array on a dielectric substrate. The theoretical model with numerical predictions predicted the results in good agreement with our experiments on the plasma FSS. Theoretically, we used Flouquets theorem to connect the elements. We determined the transmission and reflection characteristics of the plasma FSS as a function of plasma density. We utilized frequencies from around 900 MHz to 12 GHz with a plasma density around 2 GHz. We pulsed the plasma tubes to continuously vary the plasma density and observed the tunability of the reflection and transmission of electromagnetic waves. As the plasma density decays, the amount of transmitted electromagnetic energy increased as expected. However, at the electromagnetic signals at frequencies well above the plasma frequency, the plasma FSS was transparent. We also rotated the polarization of the transmitting antenna by 90° and produced a similar, but reduced effect.

We modeled an array of plasma FSSs. Similarly, we made the plasma FSS in the laboratory. Our theory and experiment were in close agreement. The plasma FSS is unique and new to the field of electromagnetic filtering. Others have developed the FSS filters using metal and dielectrics, but we are the first to use the plasma and the reconfigurability that it offers. The potential payoff for this technology is high, and the risk is moderate. It is moderate since we have developed plasma antennas with transmitters, but the plasma FSS is in some ways easier to develop since they do not require transmitters.

The plasma FSS can shield antennas, military electronics and radar systems in a tunable way. If no shielding is needed, turning the plasmas OFF causes the shield to be invisible. Plasma FSS allows users to filter out any undesirable radiation, but at the same time enabling the operations outside that band. The potential for technology transfer is significant since the plasma FSS can be tuned to filter out the unwanted radiation from commercial products or tuned to filter electromagnetic emissions to meet the FCC electromagnetic compatibility requirements.

II. Theoretical Calculations and Numerical Results

A. Model Definition

We consider an FSS dipole array as shown in Fig. 1. The structure consists of a periodic array of vertically aligned scattering elements. In traditional FSS structures, the scattering elements would be made of some material possessing a good electrical conductivity (and, thus, high reflectivity).

Fig. 1 shows the schematic representation of an FSS dipole array. This sketch illustrates a finite section of an FSS dipole. The array elements are the vertically aligned rectangular regions. For convenience of analysis, the array is assumed to extend infinitely in the plane.

For a plasma FSS structure, we imagine a scattering element to consist of gaseous plasma contained in a tube. The purpose of the present investigation is to determine the electromagnetic scattering properties of the array as a function of the reflectivity of the plasma elements. The horizontal lines on each scattering element, as shown in Fig. 1, indicate the way in which the scattering elements are divided into segments for the purpose of defining the current modes as will be discussed shortly.

Manuscript received November 9, 2005; revised December 6, 2005.

T. Anderson and I. Alexeff are with the University of Tennessee, Knoxville, TN 37996 USA and also with Haleakala R&D, Inc., Brookfield, MA 01506 USA.

J. Raynolds is with Haleakala R&D, Inc., Brookfield, MA 01506 USA.

E. Farshi, E. P. Pradeep, and J. Hulloli are with the University of Tennessee, Knoxville, TN 37996 USA.

S. Parameswaran is with Williams-Sonoma, Inc., Memphis, TN 38118 USA.

Color versions of one or more of the figures in this paper are available online at http://ieeexplore.ieee.org.

Digital Object Identifier 10.1109/TPS.2007.892676

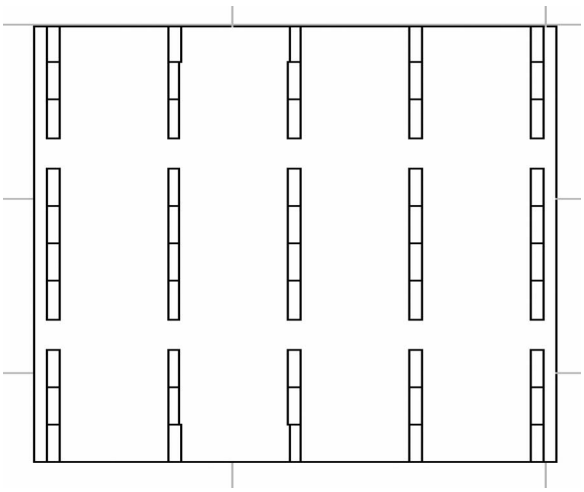

Fig. 1. Schematic representation of an FSS dipole array. This sketch illustrates a finite section of an FSS dipole array. The array elements are the vertically aligned rectangular regions. For convenience of analysis, the array is assumed to extend infinitely in the plane.

B. Method of Calculation

The response (reflection and transmission) of the plasma FSS is calculated in two stages. 1) We begin by calculating the response for a perfectly conducting structure. 2) Then, we scale the reflectivity by a function that depends on the incident frequency and the plasma frequency so as to account for the scattering properties of the plasma. Details of these two steps will now be presented.

III. Periodic Moment Method

In the first stage of calculation, we use the periodic moment method as described in the book by Munk [1]. The elements are approximated as thin flat wires. The scattered electric field produced by an incident plane wave of a single frequency is given by

$$\overline{E}(\overline{R}) = -I_A \frac{Z}{2D_x D_y} \times \sum_{k=-\infty}^{\infty} \sum_{n=-\infty}^{\infty} \frac{e^{-j\beta \overline{R} \bullet \hat{r}_{\pm}}}{r_y} \times \left[({}_{\perp}\hat{n}_{\pm})({}_{\perp}P) + ({}_{\parallel}\hat{n}_{\pm})({}_{\parallel}P) \right]. \quad (1)$$

The quantities in this equation are defined as follows. The quantity I_A is the current induced in a single element by the incident plane wave (see Munk [1, p. 106]), Z is the impedance of the medium which we take to be free space ($Z = 377\ \Omega$), $\overline{R}$ is the position vector of the observation point, and the scattering vector is defined by

$$\hat{r}_{\pm} = \hat{x} r_x \pm \hat{y} r_y + \hat{z} r_z \quad (2)$$

with

$$r_x = s_x + k\frac{\lambda}{D_x} \quad r_z = s_z + n\frac{\lambda}{D_z} \quad (3)$$

and

$$r_y = \sqrt{1 - \left(s_x + k\frac{\lambda}{D_x}\right)^2 - \left(s_z + n\frac{\lambda}{D_z}\right)^2}. \quad (4)$$

In these equations, s_x and s_z are the components of the unit vector specifying the direction of the incident plane wave. We assume that the array lies in the $x-z$ plane, with repeat distances D_x and D_z and the directions $\pm\hat{y}$, indicate the forward and back scattering directions, respectively. Note that for sufficiently high values of the integers n and k, the scattering vector component r_y becomes imaginary corresponding to evanescent modes.

The remaining quantities (in the square brackets of the expression for the scattered field) are related to the way in which the incident electric field generates a voltage in an array element as is described in detail in Munk's book [1, pp. 95–100]. The voltage induced in a scattering element by the incident field is given by

$$V(\overline{R}) = \overline{E}(\overline{R}) \bullet \hat{p} P \quad (5)$$

where $\overline{E}(\overline{R})$ is the electric field vector of the incident plane wave, $\hat{p}$ is a unit vector describing the orientation of the scattering element, and P is the pattern function for the scattering element and is defined by

$$P = \frac{1}{I^t(\overline{R})} \int_{\text{Element}} I^t(l) e^{-j\beta l \hat{p} \bullet \hat{s}} dl \quad (6)$$

where $I^t(l)$ is the current distribution on the element located at $\overline{R}$, $I^t(\overline{R})$ is the current at the terminals of the scattering element (e.g., at the center of a dipole antenna), $\hat{s}$ is the unit vector denoting the plane wave incident direction, and $\beta = 2\pi/\lambda$ is the wavenumber. The unit vectors ${}_{\perp}\hat{n}$ and ${}_{\parallel}\hat{n}$, which describe the electric field polarization, are defined by

$${}_{\perp}\hat{n} = \frac{-\hat{x} r_z + \hat{z} r_x}{\sqrt{r_x^2 + r_z^2}} \quad (7)$$

and

$${}_{\parallel}\hat{n} = {}_{\perp}\hat{n} \times \hat{r} = \frac{1}{\sqrt{r_x^2 + r_z^2}} \left[-\hat{x} r_x r_y + \hat{y}\left(r_x^2 + r_z^2\right) - \hat{z} r_y r_z \right]. \quad (8)$$

The quantities ${}_{\perp}P$ and ${}_{\parallel}P$ are given by multiplying the pattern function by the appropriate direction cosine: ${}_{\perp}P = \hat{p} \bullet {}_{\perp}\hat{n} P$ and ${}_{\parallel}P = \hat{p} \bullet {}_{\parallel}\hat{n} P$. The effective terminal current I_A, which enters the equation for the scattered electric field, is obtained from the induced voltage and the impedance as

$$I_A = \frac{V}{Z_A + Z_L} \quad (9)$$

where Z_L is the self-impedance of the scattering element and Z_A is the impedance of the array (see [2, eq. 4.69]).

As in all moment methods, some approximation must be made regarding the detailed current distribution on the scattering elements. In order to calculate the pattern function, we

assume the current distribution to be a superposition of current modes. The lowest order mode is taken to be a sinusoidal distribution of the form:

$$I_0(z) = \cos(\pi z/l) \tag{10}$$

where we have assumed the scattering element to be a conductor of length l centered at the origin. Thus, the lowest order mode corresponds to an oscillating current distribution of wavelength $\lambda = 2l$. This lowest order mode gives rise to a radiation pattern equivalent to a dipole antenna with a current source at the center of the dipole. In effect, this mode divides the scattering elements in Fig. 1 into two segments. The next two higher order modes are constructed by dividing each half of the scattering element into two more segments. These modes are written as

$$I_{1,2}(z) = \cos\left[2\pi(z \mp l/4)/l\right]. \tag{11}$$

Physically, these modes correspond to the current distributions of wavelength $\lambda = l$ centered at $\pm l/4$. Thus, the construction of the first three current modes naturally divides the scattering elements into four segments as indicated by the horizontal lines in Fig. 1. The solution of the problem is then obtained by solving a matrix problem to determine the coefficients of the various modes in the expansion of the currents. For the frequencies considered in this paper, only the lowest order mode was required, making the calculations extremely fast.

We now turn to a discussion of the scattering properties of a partially conducting plasma element.

A. Scattering From a Partially Conducting Cylinder

In order to calculate the reflection from an array of plasma elements, we make the physically reasonable assumption that (to first order) the induced current distribution in a partially conducting plasma differs from that of a perfectly conducting scattering element only to the extent that the amplitude is different. In the limit of high conductivity, the current distribution is the same as for a perfect conductor, and in the limit of zero conductivity, the current amplitude is zero.

The scattered electric field is directly proportional to the induced current on the scattering element. In turn, the reflectivity is thus directly proportional to the square of the induced current in the scattering element. Thus, to find the reflectivity of the plasma array, we determine the functional dependence of the induced squared current versus the electromagnetic properties of the plasma and scale the reflectivity obtained for the perfectly conducting case accordingly.

In order to obtain the scaling function for the squared current, we consider the following model problem. We solve the problem of scattering from an infinitely extended dielectric cylinder possessing the same dielectric properties as a partially ionized collisionless plasma. We thus assume the dielectric function for the plasma to take the following form:

$$\varepsilon(\omega) = 1 - \frac{\nu_p^2}{\nu^2} \tag{12}$$

where ν is the frequency of the incident electromagnetic wave and ν_p is the plasma frequency defined by

$$\nu_p = \frac{1}{2\pi}\sqrt{\frac{4\pi n e^2}{m}} \tag{13}$$

where n is the density of the ionized electrons, and e and m are the electron charge and mass, respectively. A good conductor is characterized by the limit of large plasma frequency in comparison to the incident frequency. In the limit in which the plasma frequency vanishes, the plasma elements become completely transparent.

We now turn to the solution of the problem of scattering from a partially conducting cylinder. The conductivity and, thus, the scattering properties of the cylinder are specified by the single parameter ν_p. We must solve the wave equation for the electric field:

$$\nabla^2 E = \frac{1}{c^2}\frac{\partial^2 D}{\partial^2 t} \tag{14}$$

subject to the boundary conditions that the tangential electric and magnetic fields must be continuous at the cylinder boundary. We consider the scattering resulting from the interaction of the cylinder with an incident plane wave of a single frequency. Therefore, we assume all fields to have the harmonic time dependence:

$$e^{-i\omega t}$$

where $\omega = 2\pi\nu$ is the angular frequency. We are adopting the physics convention for the time dependence. Personnel more familiar with the electrical engineering convention can easily convert all subsequent equations to that convention by making the substitution $i \to -j$.

Next, we assume the standard approximation relating the displacement field to the electric field via the dielectric function:

$$D(\omega) = \varepsilon(\omega)E(\omega). \tag{15}$$

By imposing a cylindrical symmetry, the wave equation takes the form of Bessel's equation:

$$\frac{\partial^2 E}{\partial^2 \rho} + \frac{1}{\rho}\frac{\partial E}{\partial \rho} + \frac{1}{\rho^2}\frac{\partial^2 E}{\partial \varphi^2} + \varepsilon k^2 E = 0 \tag{16}$$

where $k = \omega/c$ and (ρ, φ) are the cylindrical polar coordinates. The general solution of this equation consists of linear combinations of products of Bessel functions with complex exponentials. The total field outside the cylinder consists of the incident plane wave plus a scattered field of the form:

$$E_{\text{out}} = e^{ik\rho\cos\varphi} + \sum_{m=-\infty}^{\infty} A_m H_m(k\rho) e^{im\varphi} \tag{17}$$

where A_m is a coefficient to be determined and $H_m(k\rho) = J_m(k\rho) + iY_m(k\rho)$ is the Hankel function that corresponds to the outgoing cylindrical scattered waves. The field inside the

cylinder contains only the Bessel functions of the first kind since it is required to be finite at the origin:

$$E_{\text{in}} = \sum_{m=-\infty}^{\infty} B_m J_m\left(k\rho\sqrt{\varepsilon}\right) e^{im\varphi}. \tag{18}$$

To facilitate the determination of the expansion coefficients A_m and B_m, we write the incident plane wave as an expansion in Bessel functions [2]:

$$e^{ik\rho\cos\varphi} = \sum_{m=-\infty}^{\infty} i^m J_m(k\rho). \tag{19}$$

To enforce continuity of the electric field at the boundary of the cylinder, we set

$$E_{\text{in}}(\rho = a, \varphi) = E_{\text{out}}(\rho = a, \varphi) \tag{20}$$

where we have assumed the cylinder to have a radius a. The next boundary condition is obtained by imposing the continuity of the magnetic field. From one of Maxwell's equations (Faraday's law), we obtain

$$\overline{H} = -i(1/k)\nabla \times \overline{E}. \tag{21}$$

Up to this point, we have tacitly assumed that the electric field is aligned with the cylinder axis (TM polarization). This is the only case of interest since the scattering of the TE wave is minimal. The tangential component of the magnetic field is thus

$$H_\varphi = -i(1/k)\left[-\frac{\partial E_z}{\partial \rho}\right]. \tag{22}$$

By imposing the continuity of this field along with the continuity of the electric field, we obtain the following set of equations that determine the expansion coefficients:

$$i^m J_m(ka) + A_m H_m(ka) = B_m\left(ka\sqrt{\varepsilon}\right) \tag{23}$$

and

$$i^m J'_m(ka) + A_m H'_m(ka) = B_m J'_m\left(ka\sqrt{\varepsilon}\right)\sqrt{\varepsilon} \tag{24}$$

where the primes on the Bessel and Hankel functions imply a differentiation with respect to the argument.

These equations are easily solved for the expansion coefficients:

$$A_m = \frac{-i^m\left(\sqrt{\varepsilon}J_m(ka)J'_m(ka\sqrt{\varepsilon}) - J'_m(ka)J_m(ka\sqrt{\varepsilon})\right)}{\left(\sqrt{\varepsilon}H_m(ka)J'_m(ka\sqrt{\varepsilon}) - H'_m(ka)J_m(ka\sqrt{\varepsilon})\right)} \tag{25}$$

and

$$B_m = \frac{i^m\left(J_m(ka)H'_m(ka) - J'_m(ka)H_m(ka)\right)}{H'_m(ka)J_m(ka\sqrt{\varepsilon}) - \sqrt{\varepsilon}H_m(ka)J'_m(ka\sqrt{\varepsilon})}. \tag{26}$$

Inspection of these coefficients shows that in the limit $\varepsilon \to 1$ (i.e., zero plasma frequency), we obtain $A_m \to 0$ and $B_m \to i^m$. Thus, in this limit, the scattered field vanishes and the field inside the cylinder simply becomes the incident field as expected.

The opposite limit of a perfectly conducting cylinder is also established fairly easily, but requires somewhat more care. Consider first the field inside the cylinder, which must vanish in the perfectly conducting limit. A typical term in the expansion of the electric field inside the cylinder is of the form:

$$B_m J_m\left(k\rho\sqrt{\varepsilon}\right).$$

The perfect conductivity limit corresponds to taking the limit $\nu_p \to \infty$, at fixed ν. In this limit $\varepsilon \to -\nu_p^2/\nu^2$, and thus, $\sqrt{\varepsilon} \to i\nu_p/\nu$. For large imaginary argument, the Bessel functions diverge exponentially. Therefore, we can see

$$B_m J_m\left(k\rho\sqrt{\varepsilon}\right) \to O\left(\frac{\nu}{\nu_p}\right) \to 0. \tag{27}$$

Lastly, we must establish that the tangential electric field just outside the cylinder vanishes in the perfect conductivity limit as expected. Using the fact that the Bessel functions diverge exponentially for large imaginary argument gives the following limit for the scattered wave expansion coefficient:

$$A_m \to \frac{-i^m J_m(ka)}{H_m(ka)}. \tag{28}$$

Thus, a typical term in the expansion for the scattered wave, evaluated just outside the cylinder, has the following limit:

$$A_m H_m(ka) \to -i^m J_m(ka) \tag{29}$$

which exactly cancels the corresponding term in the expansion of the incident plane wave.

B. Scaling Function

We now wish to use the results from the analysis of the scattering from a partially conducting cylinder to obtain a reasonable approximation to the scattering from a partially conducting plasma FSS array based on the computed results for a perfectly conducting array.

We proceed based on the following observations/assumptions. 1) The reflectivity of the plasma FSS array is determined entirely in terms of the scattered field in contrast to the transmitted field, which depends on both the incident and scattered fields. 2) The shape of the current modes on the partially conducting (plasma) FSS array is the same as for the perfectly conducting array. 3) The only difference between the partially conducting and perfectly conducting arrays is the amplitude of the current modes.

We therefore conclude that the reflectivity of the plasma FSS can be determined from that of the perfectly conducting array by scaling the reflectivity of the perfectly conducting array by some appropriately chosen scaling function. This conclusion follows from the fact that the reflectivity is directly proportional to the squared amplitude of the current distribution on the scattering elements.

We obtain the scaling function by making the following approximation. We assume that the amplitude of the current

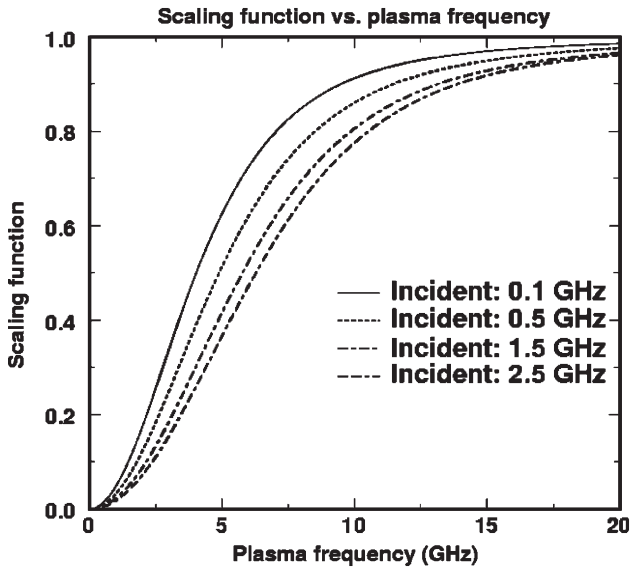

Fig. 2. Scaling function versus plasma frequency for several values of the incident frequency. This function was obtained from the solution of the problem of scattering from a partially conducting infinitely long cylinder as discussed in the text.

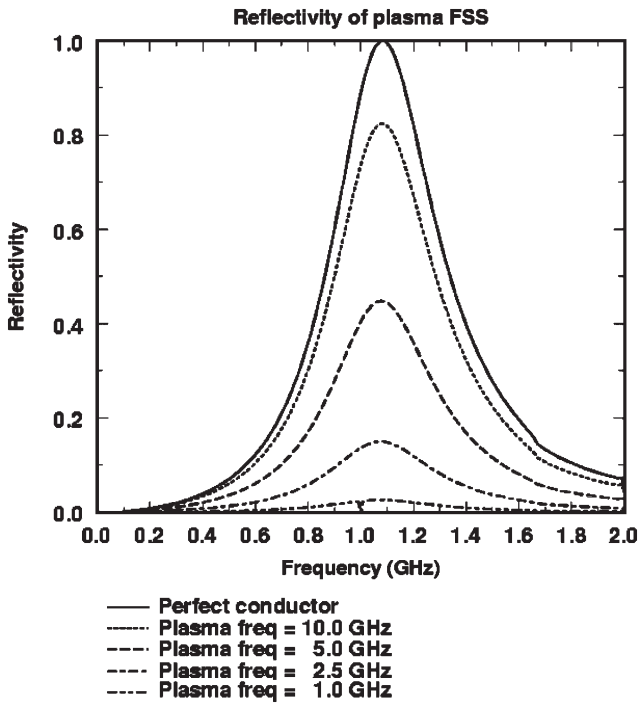

Fig. 3. Calculated reflectivity of a dipole plasma FSS array for several values of the plasma frequency. The results for the perfectly conducting case were obtained using the periodic moment method. Results for the partially conducting plasma FSS were obtained by scaling the perfectly conducting results using the scaling function in Fig. 2.

on a finite scattering segment in an FSS array scales with the plasma frequency in the same way as that for the isolated infinitely long cylinder.

We define the scaling function as

$$S(\nu, \nu_p) = 1.0 - |E_{\text{out}}|^2 \tag{30}$$

where E_{out} is the total tangential electric field evaluated just outside of the cylinder. Clearly, from the results of the previous section, the scaling function takes on the values:

$$0.0 \leq S(\nu, \nu_p) \leq 1.0 \tag{31}$$

for fixed incident frequency ν, as the plasma frequency takes on the values:

$$0.0 \leq \nu_p \leq \infty. \tag{32}$$

This function is plotted versus ν_p for several values of the incident frequency in Fig. 2. This figure shows the plot of the scaling function versus plasma frequency for several values of the incident frequency. This function was obtained from the solution of the problem of scattering from a partially conducting infinitely long cylinder as discussed in the text.

IV. Results

We now present the results for two cases: 1) an array designed to have a well-defined reflection resonance near 1 GHz (a band stop filter) and 2) an array designed to operate as a good reflector for similar frequencies.

A. Switchable Band Stop Filter

The first array is shown in Fig. 1. Each scattering element is assumed to be 15 cm in length and 1 cm in diameter. The vertical separation is taken to be 18 cm, while the lateral separation is taken to be 10 cm. The results for the perfectly conducting case along with those for several values of the plasma frequency are presented in Fig. 3. A well-defined reflectivity resonance exists at 1 GHz. This result indicates that an appreciable reflection occurs only for plasma frequencies above 2.5 GHz. The results in Fig. 3 illustrate the essence of the plasma FSS: A highly reflective band stop filter can be achieved, which can be switched on and off simply by controlling the properties of the plasma.

Fig. 3 shows the calculated reflectivity of a dipole plasma FSS array for several values of the plasma frequency. The results for the perfectly conducting case were obtained using the periodic moment method. Results for the partially conducting plasma FSS were obtained by scaling the perfectly conducting results using the scaling function in Fig. 2.

B. Switchable Reflector

Next, we consider a structure designed to be a switchable reflector. By placing the scattering elements close together, we obtain a structure that acts as a good reflector for sufficiently high frequencies. Such a structure is shown in Fig. 4. The length, diameter, and the vertical and lateral spacings are 10, 1, 11, and 2 cm, respectively.

The calculated reflectivity for the perfectly conducting case as well as for several values of the plasma frequency is presented in Fig. 5. For frequencies between 1.8 and 2.2 GHz, the structure operates as a switchable reflector. In other words, by changing the plasma frequency from low to

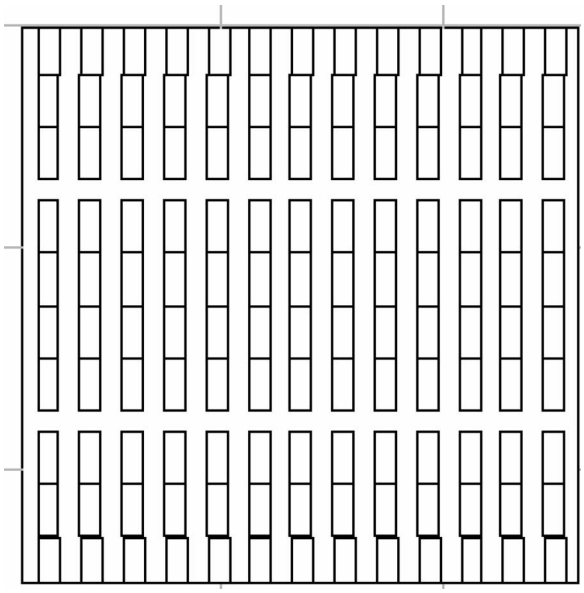

Fig. 4. Illustration of a switchable reflector. The scattering elements are chosen to be 10 cm in length and 1 cm in diameter. The vertical spacing is 11 cm, and the horizontal spacing is 2 cm.

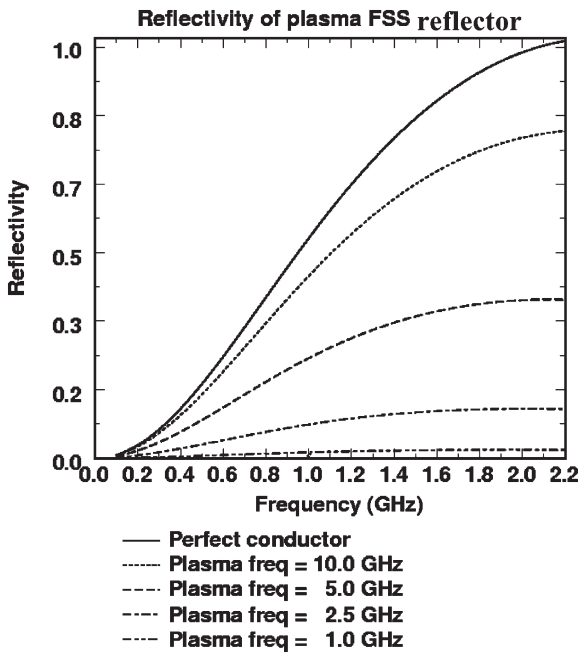

Fig. 5. Reflectivity for switchable plasma reflector illustrated in Fig. 4. For frequencies between 1.8 and 2.2 GHz, the structure operates as a good reflector for sufficiently high values of the plasma frequency.

high values, the reflector goes from perfectly transmitting to highly reflecting.

C. Experimental Plasma FSS Work

Metal FSSs were built (Fig. 6). Experimental work on plasma FSS (Fig. 7) began by letting the tubes spaced within a wavelength apart be pulsed and letting them decay to observe the filtering characteristics with plasma density (see Figs. 8 and 13). Then, the plasma FSSs were built (Figs. 8, 10–12). The tubes are activated by wire sections connected to the end

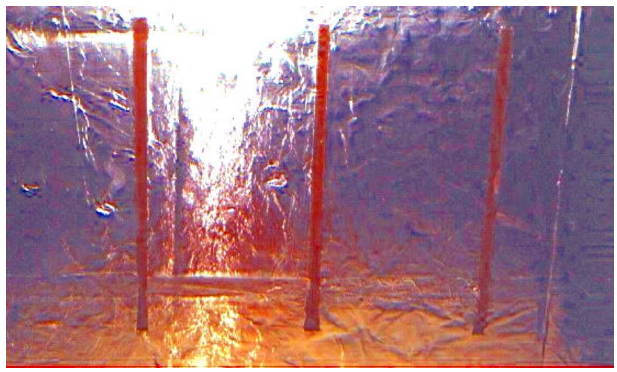

Fig. 6. Foil-on-cardboard filter with a passband at 960 MHz.

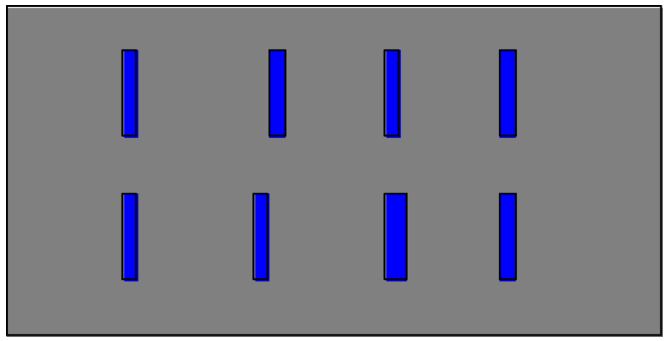

Fig. 7. In general, the plasma FSS will be an array of FSS elements with plasma (blue) embedded in a dielectric (gray).

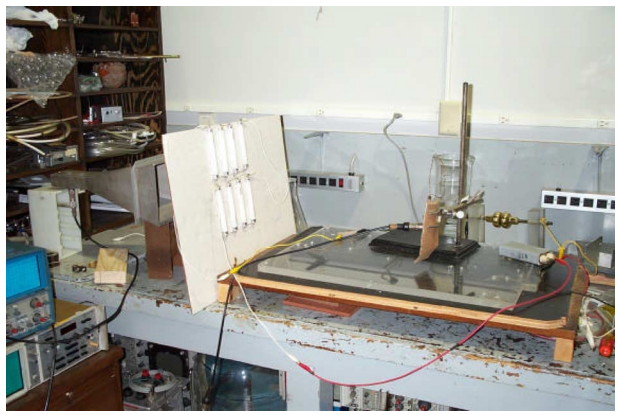

Fig. 8. Is a photograph of the lab setup showing the built plasma dipole FSS with the horn receiver antenna.

of the light tubes. We do not have a scattering from these wires because the electric field is perpendicular. The noise was not particularly worse for our system, and it is a few decibels above the metal antenna. However, when the system was deenergized, the reflected signal dropped by 20 dB. In other words, the reflected signal dropped by over a factor of 100 [3]. The experimental plot in Fig. 9 is compared well with the theoretical plot in Fig. 11. Differences are due mainly that the theoretical plot was an infinite array and the experimental plot was finite. The peak resonance in the theoretical and experimental plots was very close, and the subpeaks in the experimental plot are due to the finite size of the array.

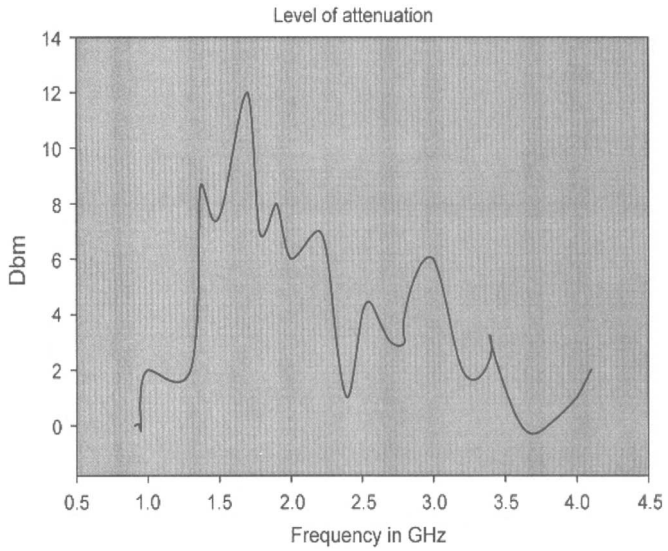

Fig. 9. Tubes are 10.16- and 12.7-cm long, metal ends included. They are 5.08 cm apart horizontally. One inch apart vertically. The first peak corresponds to a frequency resonance. Here, we are talking about the attenuation of the transmitted signal.

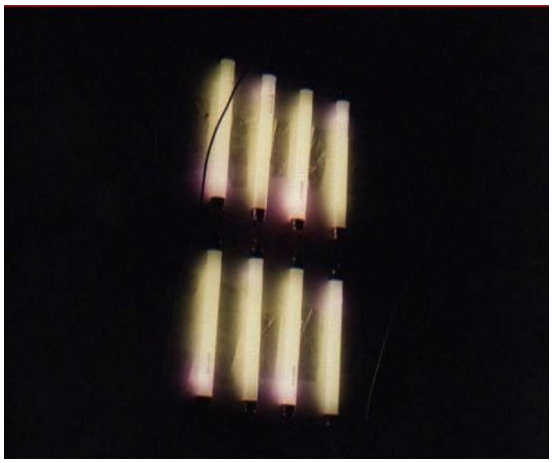

Fig. 10. Plasma FSS turned on.

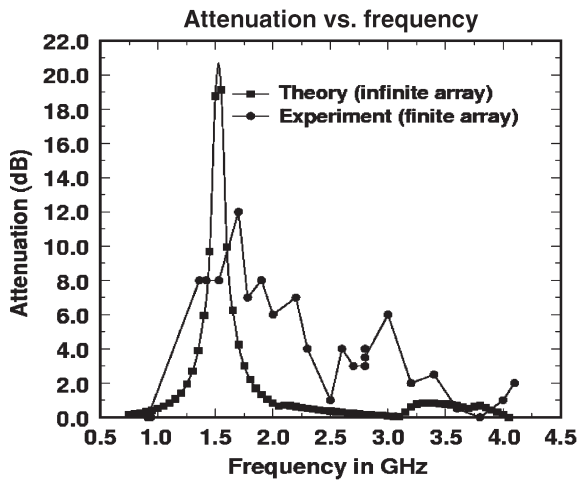

Fig. 11. Theoretical and experimental plots superimposed. The same dimensions used here for theoretical plot as in the experimental prototype in Fig. 7, except that the theoretical array is infinite and the experimental array is finite. Here, we are talking about the attenuation of the transmitted signal.

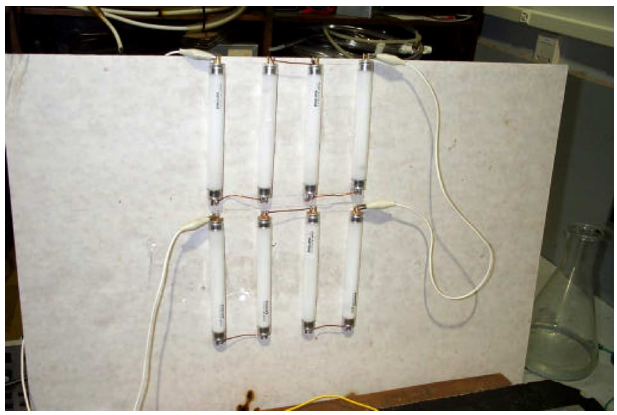

Fig. 12. Shows the plasma dipole FSS.

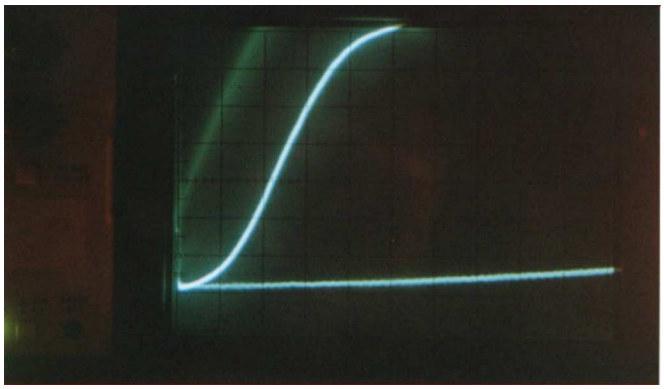

Fig. 13. In the photograph, run 4, the transmitting antenna was emitting at 0.9 GHz. There was a cutoff (reflection) initially, but as the plasma decayed, we see a transmission through the plasma FSS.

Since the horizontal control wires in Fig. 12 are horizontal, no induced voltage will be present in them. However, the element current can continue right up to the control wires and turn 90°, producing very strong currents on these wires unless they are stopped by a choke. We will probably get a sharper resonance if the currents on the control wires were suppressed. We will use a choke in our next experiments to see its effect for our future paper. However, probably, we do not have the scattering from the wires because the electric field is perpendicular, and the tubes all have the same induced voltage for plane wave perpendicular.

V. Conclusion

A theory of plasma FSSs has been presented, and two structures have been analyzed. The theory is based on the physically reasonable assumption that the current modes induced in the plasma scattering elements have the same form, but different amplitude from those for a perfect conductor. The reflectivity of the structure is directly proportional to the squared amplitude of the current distribution induced in the scattering elements by the incident radiation. Based on this observation, we conclude that the reflectivity of a plasma FSS structure can be obtained from that for a perfectly conducting structure by scaling the reflectivity with an appropriately chosen scaling function.

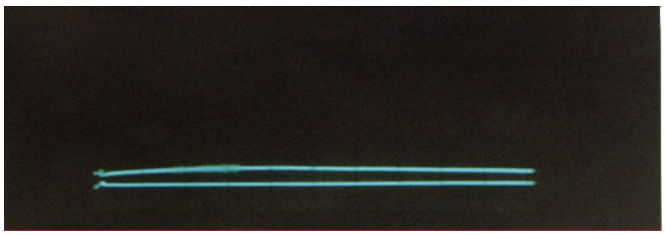

Fig. 14. This photograph demonstrates the transmitting antenna emitting at 4 GHz, with an oscilloscope scale of 0.1 ms/cm. In this case, the electromagnetic waves go through the plasma FSS as expected.

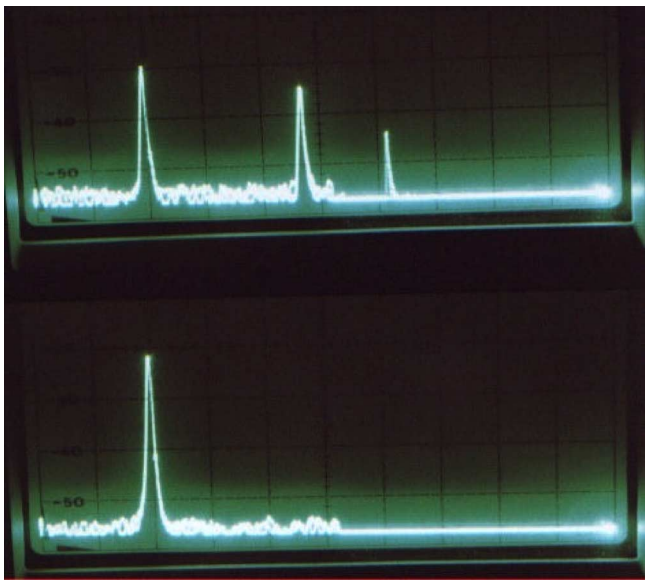

Fig. 15. Putting in the passband between transmitter and receiver removes the second and higher harmonics. (2 dB per square).

The scaling function was defined based on the results of the exactly solvable model of scattering from an infinitely long partially conducting cylinder. The approximation was made that the scaling of the current amplitude versus plasma frequency in the plasma FSS array should be the same as for an isolated infinitely long partially conducting cylinder.

The reflectivity for a perfectly conducting FSS array, obtained by the periodic moment method, was then scaled to obtain the reflectivity of the plasma FSS array versus plasma frequency. Two cases were considered: 1) a switchable bandstop filter and 2) a switchable reflector. The results of these calculations support the notion that the switchable FSS filtering behavior can be obtained with the use of the plasma FSS.

Experimental work on plasma FSS began by letting the tubes spaced within a wavelength apart be pulsed and letting them decay to observe the filtering characteristics with the plasma density (see Figs. 13 and 15). Metal FSSs were built (Fig. 6). Then, plasma FSSs were built (Figs. 8, 10–12). The experimental plot in Fig. 9 is compared well with the theoretical (together experimental) plot in Fig. 11.

The superposition of the experimental and theoretical works given in Fig. 11 shows a good agreement. Differences are due mainly that the theoretical plot was an infinite array and the experimental plot was finite. The peak resonance in the theoretical and experimental plots was very close, and the subpeaks in the experimental plot are due to the finite size of the array.

As can be seen by the photographs, changing the transmitting frequency also causes the FSS to reflect and conduct. At 0.9 GHz, we see an initial reflection, but as the plasma deionizes, the signal penetrates the FSS. Also, when the frequency is raised to 4 GHz (Fig. 14), the emissions go through the FSS as predicted. Some of these plasma antenna applications have been patented [4], [5].

REFERENCES

[1] B. A. Munk, *Frequency Selective Surfaces*. New York: Wiley-Interscience, 2000.
[2] L. Eyges, *The Classical Electromagnetic Field*. New York: Dover, 1980, p. 320.
[3] I. Alexeff, T. Anderson, S. Parameswaran, E. P. Pradeep, J. Hulloli, and P. Hulloli, "Experimental and theoretical results with plasma antennas," *IEEE Trans. Plasma Sci.*, vol. 34, no. 2, pp. 166–172, Apr. 2006.
[4] T. R. Anderson and K. Victor, "Multiple plasma antenna," U.S. Patent 5 963 169, Oct. 5, 1999. issued by the United States of America as Represented by the Secretary of the Navy (Washington, DC).
[5] E. G. Norris, I. Alexeff, and T. Anderson, "Reconfigurable plasma antenna," U.S. Patent 6 369 763, Apr. 9, 2002.

Ted Anderson received the Ph.D. degree in physics from New York University, New York, in 1986.

He was with the Naval Undersea Warfare Center for 12 years. He has taught at the University of Connecticut for 12 years and Rensselaer Polytechnic Institute for 16 years. He is a Research Professor with University of Tennessee, Knoxville. He is a world leader in plasma antenna technology with many publications and over 20 patents on plasma technology. He is the Founder and CEO of Haleakala R&D, Inc., Brokfield, MA.

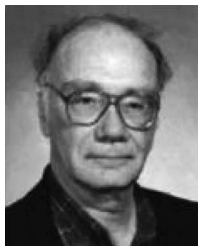

Igor Alexeff (M'72–SM'76–F'81) received the B.S. degree in physics from Harvard University, Cambridge, MA, in 1952 and the Ph.D. degree in nuclear physics from University of Wisconsin, Madison, in 1959.

He is currently a Professor Emeritus at the University of Tennessee, Knoxville, and is also with Haleakala R&D, Inc., Brookfield, MA. He has been working in plasma and microwave engineering for over 50 years. He has a patent on the Orbitron Microwave Maser that has operated up to 1 THz (1/3 mm). He is an Author and a Coeditor of the book *High Power Microwave Sources* (Norwood, MA: Artech House). He has over 100 refereed publications and over ten patents. He has spent a considerable time recently on plasma stealth antennas and is listed on several patents issued to the ASI Technology Corporation. He has worked with the Westinghouse Research Laboratory on nuclear submarines, at the Oak Ridge National Laboratory in controlled thermonuclear fusion, and at the University of Tennessee in industrial plasma engineering. He has worked overseas for extended periods in Switzerland, Japan, India, South Africa, and Brazil.

Dr. Alexeff was a Cofounder of the IEEE Nuclear and Plasma Sciences Society, and was the President of that society from 1999 to 2000. He is a Fellow of the American Physical Society. He also passed the Tennessee State License Exam, and is a registered Professional Engineer.

James Raynolds received the Doctoral degree in physics from Ohio State University, Columbus.

During his stay with University of Michigan as a Postdoctoral Researcher, he held a joint appointment with the General Motors Research and Development Center in Warren Michigan. His research focus during this time was the study of interfacial adhesion in intermetallic composites as well as the development of new computational methods. During this time, his research focused on the use of heavily doped semiconductors as well as micrometer scale passive antenna arrays as components for thermophotovoltaic energy conversion systems. He consults with Haleakala R&D, Inc., Brookfield, MA.

Esmaeil Farshi received the Ph.D. degree in plasma physics and Dr. Eng. degree in energy systems.

He is a Research Professor with University of Tennessee, Knoxville. He has worked as a Scientist and a Professor in Europe, Japan, Russia, and the USA. He is interested in high-temperature plasma, tokamak, fusion, kinetic theory, RF, and microwave.

Sriram Parameswaran received the B.S. degree in electrical engineering from the University of Madras, Chennai, India, the M.S. degree in electrical engineering, and the M.B.A. degree in logistics from the University of Tennessee, Knoxville, under the guidance of Dr. I. Alexeff.

He worked under various projects, which include plasma sterilazation, ball lightning, and plasma antennas. He is currently a Project Engineer at Williams-Sonoma, Inc., Memphis, TN. He contributed to this work while at the University of Tennessee.

Mr. Parameswaran received the IEEE Nuclear and Plasma Sciences Society graduate scholarship award for the year 2004.

Eric P. Pradeep (S'05) was born in Coimbatore, India. He received the B.S. degree in electrical and electronics engineering from University of Madras, Madras, India. He is currently working toward the M.S. degree at University of Tennessee, Knoxville.

He has been working for Dr. I. Alexeff as a Graduate Research Assistant in the Microwave and Plasma Laboratory for about two years.

Jyothi Hulloli received the B.S. degree in electrical engineering from Karnataka University, Karnataka, India. She is currently working toward the M.B.A. degree at University of Tennessee, Knoxville.

After receiving the B.S. degree, she worked as a Research Associate with one of the top engineering colleges of India. She is currently working as a Graduate Assistant with Dr. I. Alexeff to assist in developing business plans for plasma devices.